Vascular Imaging of Solid Tumors in Rats with a Radioactive Arsenic-Labeled Antibody that Binds Exposed Phosphatidylserine

Marc Jennewein,[1,2] Matthew A. Lewis,[2,3] Dawen Zhao,[2] Edward Tsyganov,[2] Nikolai Slavine,[2] Jin He,[3,4] Linda Watkins,[3,4] Vikram D. Kodibagkar,[2] Sean O'Kelly,[6] Padmakar Kulkarni,[2] Peter P. Antich,[2] Alex Hermanne,[5] Frank Rösch,[1] Ralph P. Mason,[2,3] and Philip E. Thorpe[3,4]

Abstract

Purpose: We recently reported that anionic phospholipids, principally phosphatidylserine, become exposed on the external surface of vascular endothelial cells in tumors, probably in response to oxidative stresses present in the tumor microenvironment. In the present study, we tested the hypothesis that a chimeric monoclonal antibody that binds phosphatidylserine could be labeled with radioactive arsenic isotopes and used for molecular imaging of solid tumors in rats.

Experimental Design: Bavituximab was labeled with ^{74}As (β^+, $T_{1/2}$ 17.8 days) or ^{77}As (β^-, $T_{1/2}$ 1.6 days) using a novel procedure. The radionuclides of arsenic were selected because their long half-lives are consistent with the long biological half lives of antibodies *in vivo* and because their chemistry permits stable attachment to antibodies. The radiolabeled antibodies were tested for the ability to image subcutaneous Dunning prostate R3227-AT1 tumors in rats.

Results: Clear images of the tumors were obtained using planar γ-scintigraphy and positron emission tomography. Biodistribution studies confirmed the specific localization of bavituximab to the tumors. The tumor-to-liver ratio 72 h after injection was 22 for bavituximab compared with 1.5 for an isotype-matched control chimeric antibody of irrelevant specificity. Immunohistochemical studies showed that the bavituximab was labeling the tumor vascular endothelium.

Conclusions: These results show that radioarsenic-labeled bavituximab has potential as a new tool for imaging the vasculature of solid tumors.

Imaging offers noninvasive perspective on tumor development and therapy, providing information on receptor expression, targeting, and drug pharmacokinetics. Imaging technologies include positron emission tomography (PET), single-photon emission computed tomography, MRI, ultrasound, and optical imaging, as reviewed extensively elsewhere (1, 2). Nuclear medicine approaches are particularly relevant because extremely low concentrations of tracer/reporter are permissible. Several radionuclides are in clinical use, and many more are under development (3–5). However, many isotopes decay rapidly, limiting shelf life and preventing investigation of long-term biological phenomena. A particular problem arises with antibodies, which usually have a long biological half life and do not reach optimal target to background selectivity for several days. For PET, common radionuclides, such as ^{64}Cu (18% β^+ positron branching, $T_{1/2}$ 12.7 h) or ^{86}Y (32% β^+, $T_{1/2}$ 17.8 h) have too-short half-lives for following antibody localization, whereas ^{124}I (24% β^+, $T_{1/2}$ 4.18 days) has a suitable $T_{1/2}$ but undergoes metabolic dehalogenation and release of iodine.

Arsenic radioisotopes include long-lived positron emitters having favorable characteristics for PET: ^{71}As ($T_{1/2}$ 64 h, 30% β^+, 104 keV average kinetic energy of the positrons), ^{72}As ($T_{1/2}$ 26 h, 88% β^+, 1.024 keV), and ^{74}As ($T_{1/2}$ 17.8 days, 29% β^+, 128 keV). Other arsenic isotopes are high-energy β^- emitters that could potentially be used for tumor therapy: ^{77}As ($T_{1/2}$ 38.8 h, $\bar{E}_{\beta^-}$ 226 keV) and ^{76}As ($T_{1/2}$ 26.3 h, $\bar{E}_{\beta^-}$ 1.068 keV). The decay characteristics of the arsenic isotopes that are most relevant for imaging or therapy are presented in Supplementary Table S1. ^{74}As was used in some of the earliest radionuclide imaging studies for the development of PET, at that time, called positrocephalography (6). However, inefficient isotope production, difficulty in isolating pure nuclides, and lack of

effective derivatization processes handicapped the exploitation of arsenic isotopes. Radiochemistry has now evolved, and several isolation procedures for arsenic isotopes have been reported. Most recently, Jennewein and Rösch developed efficient methods for isolating pure radionuclides from irradiated GeO_2 targets on the basis of a solid phase extraction system (7, 8). Moreover, Jennewein and Rösch proposed chemistry for the effective labeling of biologically relevant molecules, as we have now exploited.

Bavituximab, a chimeric antibody targeting exposed vascular phosphatidylserine, was chosen to develop the labeling procedure and show the first *in vivo* use of arsenic isotopes for PET imaging of solid tumors. Bavituximab binds to phosphatidylserine by stabilizing a complex of two β2-glycoprotein I molecules attached to phosphatidylserine on the cell surface (9–12). Phosphatidylserine is normally tightly segregated to the internal surface of the plasma membrane in most cell types, including the vascular endothelium (10, 11, 13, 14). Phosphatidylserine asymmetry is maintained by ATP-dependent aminophospholipid translocases (Mg^{2+}-ATPase) that catalyze the transport of aminophospholipids from the external to the internal leaflet of the plasma membrane (15). Loss of phosphatidylserine asymmetry occurs during apoptosis (16), necrosis (17), cell activation (18), and transformation (19), resulting in the exposure of phosphatidylserine on the external surface of the cells. Phosphatidylserine exposure occurs when the aminophospholipid translocases become inhibited (20) or when transporters, such as scramblase (21) and floppases (22), become activated by Ca^{2+} fluxes into the cytosol (23, 24).

We previously showed that anionic phospholipids become exposed on the vascular endothelium of blood vessels in mice bearing various types of solid tumors probably in response to oxidizing stresses in the tumor (10, 11). There was no detectable exposure on vascular endothelium in normal tissues, including the ovary, a site of physiologic angiogenesis, and the pancreas, a site of high vascular permeability. Phosphatidylserine is one of the most specific markers of tumor vasculature yet discovered. The murine version of bavituximab, 3G4, retards tumor growth in multiple rodent models by stimulating host cells to bind to and destroy tumor blood vessels. Bavituximab is currently in phase I clinical trials in patients with various solid tumors.[7] Despite its proven ability to target tumor endothelium, bavituximab has not yet been explored as an imaging agent. The vascular location of phosphatidylserine ensures ready access by radiolabeled antibody in the blood. Imaging techniques could not only enable the detection of tumors and their metastases, but also verify the presence of antigen before bavituximab therapy.

In the present study, we tested the hypothesis that bavituximab can be labeled with radioactive arsenic isotopes and used for vascular targeting and molecular imaging of solid tumors in rats. Doses of bavituximab that are 10-fold below the doses that have significant vascular damaging activity were used (14) to prevent occlusion of tumor vasculature from impeding effective imaging. Clear tumor imaging was obtained by planar γ-scintigraphy and PET.

Materials and Methods

Antibodies. Bavituximab was provided by Peregrine Pharmaceuticals, Inc. Bavituximab is a chimeric antibody composed of the Fv regions of the mouse antibody 3G4 (14) and the constant regions of human IgG1. Bavituximab binds to phosphatidylserine through a cofactor protein, β2-glycoprotein I. Bavituximab recognizes rat β2-glycoprotein I as strongly as it does human β2-glycoprotein I, avoiding the need for supplementation with exogenous human β2-glycoprotein I, which is necessary in the mouse (14). Bavituximab binds to human β2-glycoprotein I with an affinity of 1.7×10^{-8} mol/L (monovalent interaction) and an avidity of $\sim 10^{-10}$ mol/L (divalent interaction) in Biacore experiments.

Hamster anti-mouse CD31 monoclonal antibody was from BD PharMingen. Secondary antibodies were from Jackson Immunoresearch Lab. Rituximab (monoclonal antibody Thera, CD20) was purchased from Roche.

Isotopes. ^{74}As for PET imaging was produced by $^{nat}Ge(p,xn)^{74}As$ reaction (E_p = 20 MeV, 3 h irradiation at 15 μA), giving a yield of ~ 370 MBq. ^{77}As for scintigraphy was produced in a no-carrier-added (nca) state via the $^{76}Ge(n,\gamma)^{77}Ge$, $T_{1/2}$ 11.30 h→β⁻→^{77}As processes in a TRIGA reactor ($\Phi = 4.0 \times 10^{13}$ n/cm²·s).

Radiochemical separations. Nuclear reactions were typically done on 100 mg of $^{nat}GeO_2$ (99.9999% grade, PURA TREM, Strem Chemicals, Inc.). Irradiated germanium oxide targets were dissolved in 5 mL $HF_{conc.}$ and extracted as described in detail previously (7), providing nca [*As]AsI_3 fixed to the solid phase of the extraction cartridge (Varian BOND ELUT ENV solid phase extraction cartridges with a sorbent mass of 50 mg and a volume of 1 mL). Excess $HF_{conc.}$ was removed with a high-pressure nitrogen flow over the cartridge for 5 min. When required for labeling, nca [*As]AsI_3 was eluted with 500 μL ethanol and concentrated to 50 μL under a gentle N_2 flow. The radioarsenic separation yield and efficacy of nca [*As]AsI_3 was >90%.

Antibody conjugation and testing. Antibodies were SATA-modified according to the protocol of Pierce Endogen (25). Deprotection of the sulfhydryl groups of the monoclonal antibody derivative using hydroxylamine was done directly before the labeling. The number of free thiol groups per antibody molecule was measured using Ellman's reagent and by comparison with cysteine-based standards. Thiolated antibody (100 μg) in PBS (3 mL, pH 7.5) was combined with the nca [*As]AsI_3 solution at 37°C for 30 min. [*As]AsI_3 couples to one SH functionality with elimination of HI as illustrated in Fig. 1. Quality control of the antibody labeling was done by HPLC, using an Agilent 1100 Series HPLC system, with an LDC/Milton Roy UV monitor III at 254 nm and a 'Gabi' NaI radiation monitor from Raytest. The HPLC column was a Bio-Silect Sec 250-5, 300 × 7.8 mm and PBS + 0.01 mol/L NaN_3 was used as solvent at a flow of 0.8 mL/min. Retention time of the *As[SATA] labeled antibodies was 11.5 ± 0.5 min. To keep the thiols from forming disulfide bridges, all solutions were kept out of contact with air and contained 1 mmol/L EDTA.

In vitro stability. The radioarsenic-labeled bavituximab was tested for possible transfer of radioarsenic to proteins present in blood plasma. This was done by incubating the labeled antibody in fetal bovine serum and examining the mixture by HPLC at various time points up to 72 h. Radioarsenic-labeled bavituximab (10 μg) in PBS (50 μL) was added to undiluted fetal bovine serum (500 μL) and incubated at 37°C. Samples (50 μL) were taken at 30 min, 24 h, 48 h, and 72 h, diluted with 200 μL water, and examined by HPLC.

Binding of bavituximab antibody to plastic-immobilized phospholipids. Phospholipids were dissolved in *n*-hexane to a concentration of 50 μg/mL. One hundred microliters of this solution were added to wells of 96-well microtiter plates. After evaporation of the solvent in air, the plates were blocked for 2 h with 1% bovine serum albumin diluted in PBS (binding buffer). Bavituximab was diluted in the binding buffer containing 10% fetal bovine serum at an initial concentration of 33 nmol/L. Serial 2-fold dilutions were prepared in the plates

(100 μL/well). The plates were then incubated for 1 h at room temperature. After washing with PBS, horseradish peroxidase goat anti-human IgG (diluted 1:2,000) was used to detect bavituximab. Secondary reagents were detected by using chromogenic substrate *O*-phenyldiamine followed by reading plates at 490 nm using a microplate reader (Molecular Devices). Binding of [^{77}As]bavituximab to phosphatidylserine-coated plates was determined using unmodified bavituximab as the positive control and [^{77}As]rituximab as the negative control. The concentrations of [^{77}As]bavituximab and unmodified bavituximab that gave half-maximal binding were determined. Because the association rate of bavituximab with phosphatidylserine on the plate is rapid and its dissociation is negligible over the time course of the experiment, the half-maximal binding concentrations allow the antigen-binding capacities of the labeled and unmodified antibodies to be compared under conditions that approximate equilibrium.

Growth of tumors. All experiments were conducted in accordance with recommendations of The University of Texas System Institutional Animal Care and Use Committee. A Dunning prostate R3327-AT1 tumor (originally provided by Dr. Peter Peschke, German Cancer Center) was excised from a donor animal (26, 27). Small pieces were implanted s.c. into the left thigh of male Copenhagen rats (Charles River) and allowed to grow to a size of 15 to 25 mm diameter.

Biodistribution and planar imaging studies. Three animals each were injected with [^{74}As]bavituximab or with [^{74}As]rituximab in PBS (5 MBq in 500 μL) into a tail vein. The animals were sedated using

isoflurane (Baxter Healthcare) and imaged on a 25.2 × 30.3 cm phosphor imaging plate (Fuji CR ST-VN, Fuji Photo Film). The photostimulable plates were read on a Molecular Dynamics Storm (Amersham Biosciences) scanner and regions of interest drawn around the tumors and upper body for quantification. In a second study, four animals injected with 3 MBq of [^{77}As]bavituximab or [^{77}As]rituximab were imaged at 48 and 72 h using a 30-min exposure time. Prior studies have established that [^{74}As]bavituximab and [^{77}As]bavituximab have identical pharmacologic variables, i.e., independent of the isotope of arsenic. In a further study, rats were injected with 3 MBq of [^{77}As]bavituximab or [^{77}As]rituximab and were sacrificed without exsanguination 48 or 72 h later. Tumors were excised and frozen, and 1-mm sections were cut. Tumor sections were autoradiographed with exposure times of 12 h for [^{77}As]bavituximab and 48 h for [^{77}As]rituximab to visualize the distribution of radioactivity within the tumors.

PET studies. Four animals each were injected with 10 MBq of [^{74}As]bavituximab or [^{74}As]rituximab in 500 μL of PBS (pH 7.4, 1 mmol/L EDTA) via a tail vein. The animals were anesthetized with isoflurane and imaged over 2 h after 24, 48, and 72 h using a small animal PET system built at University of Texas Southwestern (28, 29). The images were reconstructed using the maximum likelihood - expectation maximization (ML - EM) algorithm for three-dimensional reconstruction (28) After 72 h, the animals were sacrificed by exsanguination and perfusion via cardiac puncture under general

Fig. 1. *A,* reaction scheme for the labeling of SATA-modified antibody with radioactive arsenic isotopes. *B,* quality control of bavituximab labeling with radioactive arsenic. After a labeling time of 30 min, a sample of [^{74}As]bavituximab (20 μL) was resolved on a size-exclusion column for radio-HPLC. The UV spectrum (*top*) and corresponding radioactivity progression (*bottom*) confirm the absence of aggregates and of free ^{74}As. Labeling yield is >99.9%. *C, in vitro* stability of [^{74}As]bavituximab. [^{74}As]bavituximab was incubated in undiluted fetal bovine serum for 24, 48, and 72 h. Size exclusion radio-HPLC was done. The UV spectrum (*top*) shows a typical fetal bovine serum profile because the amount of [^{74}As]bavituximab is too small to detect. *Bottom,* graphs show the corresponding radioactivity peak. Aggregates and breakdown products were not observed, indicating that the product is stable in serum. *D,* immunoreactivity. ELISA was used to analyze the immunoreactivity of [^{77}As]bavituximab (●). Unlabeled and unmodified bavituximab was used as the positive control (○) and [^{77}As]rituximab as the negative control (▼). Little or no reduction of immunoreactivity was detected after SATA modification and radioarsenic labeling.
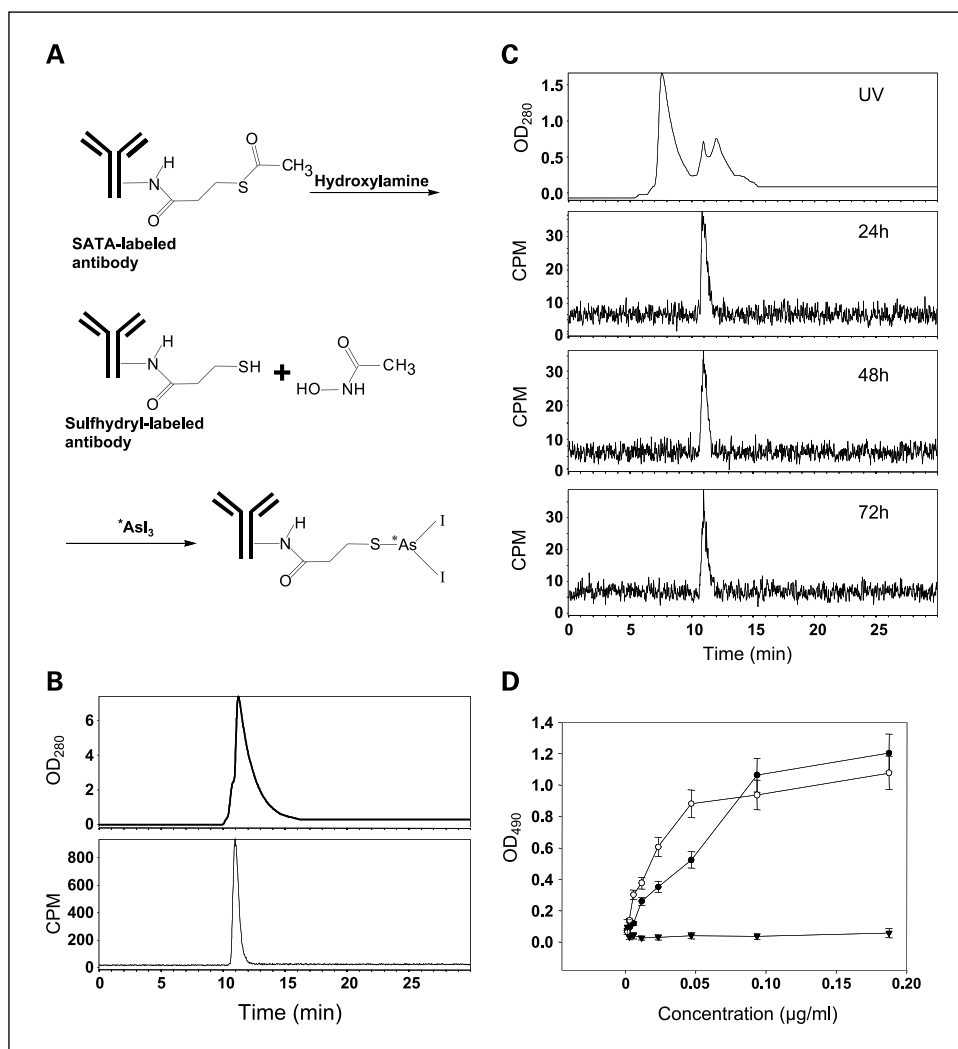
anesthesia, and major organs and tumors were collected and their radioactivity measured in a Gamma counter.

MRI. T1-weighed spin-echo MR images were obtained from rats with size-matched tumors for anatomic comparison. The images were acquired with TR/TE of 450 ms:14 ms. The acquisition matrix was 128×256 zero-filled to $512 \times 1,024$ with field of view 10×20 cm and a slice thickness of 1 mm.

Detection of localized bavituximab in tumor-bearing rats in vivo. Groups of two male Copenhagen rats (200 g weight) bearing AT1 tumors (s.c., 15 mm diameter) were injected i.v. with 1 mg bavituximab or control antibody (rituximab). Twenty four hours later, rats were anesthetized and their blood circulation was perfused with heparinized saline to clear it of free antibody, as described above. Organs and tumors were removed and snap-frozen for preparation of cryosections. Sections were fixed with 4% paraformaldehyde in PBS and blocked with PBS containing 1% bovine serum albumin. To prevent loss of phospholipids during slide processing, detergents and organic solvents were omitted from blocking and washing buffers. Chimeric IgG was detected using biotinylated goat anti-human IgG followed by Cy2-streptavidin. Vascular endothelium was detected by mouse anti-rat CD31 antibody followed by Cy3-goat anti-mouse antibody (minimally reactive with rat serum). Tumor sections derived from rats injected with rituximab served as negative controls. Single images, taken with appropriate filters for Cy2 (green) and Cy3 (red) fluorescence, respectively, were captured by digital camera and transferred to a computer. Images of 10 random fields (0.317 mm^2/field) were merged with the aid of Metaview software. When bavituximab was bound to tumor endothelium, the green and red fluorescence often merged to give a yellow color. The percentage of vessels with localized bavituximab was calculated.

Results

^{74}As and ^{77}As were produced, radiochemically separated, and transformed into the labeling synthon *AsI$_3$. Isotopes were chosen depending on the goal of each study, so that ^{74}As was used for *ex vivo* organ distribution, whole-body planar imaging (*in vivo* and *ex vivo*), and *in vivo* PET imaging. ^{77}As was used to develop the radiochemistry and labeling procedures and used to label bavituximab for whole-body planar imaging *in vivo* and biodistribution.

Babituximab was modified with SATA to introduce an average of 3.5 free thiol groups per molecule of antibody (Fig. 1A). Arsenic has a high affinity for sulfur, and AsI$_3$ is able to bind covalently to sulfhydryl groups (7). *AsI$_3$ conjugation to the SATA-modified antibodies was achieved quantitatively (Fig. 1B). The specific activity of the [*As]labeled antibodies was >100 GBq/μmol. Incubation in serum for up to 72 h did not cause release of radioarsenic from the labeled monoclonal antibody or formation of antibody fragments (Fig. 1C). Complexes of bavituximab and β2-glycoprotein I were not observed, probably because the complex is not stable in the absence of an anionic phospholipid surface upon which to dimerize. Immunoreactivity of the labeled bavituximab was verified by ELISA. Little or no loss of phosphatidylserine-binding activity was observed after SATA-modification and subsequent labeling with nca [^{77}As] AsI$_3$ (Fig. 1D). The concentration of [^{77}As]bavituximab giving half-maximal binding was less than twice that for unmodified bavituximab, indicating that the labeling procedure had caused less than a 2-fold reduction in the antigen-binding capacity of the antibody.

Rats bearing Dunning R3227-ATI prostate tumors of ~15 mm in diameter were injected i.v. with [^{74}As]bavituximab or with the isotype-matched control antibody, [^{74}As]rituximab. The radioactivity present in various organs was measured 48 and 72 h after injection. These time points were selected because they gave good tumor localization in the imaging studies below. Tumor to normal tissue ratios were highest for bavituximab at 72 h after injection, consistent with the imaging results. Tumor-to-liver and tumor-to-muscle ratios at 72 h were 22 and 470, respectively (Fig. 2A and B). Bavituximab localized to tumors to a greater extent than did the control antibody rituximab. The ratios of bavituximab to rituximab were 28 and 52 at 48 and 72 h, respectively (Fig. 2C). The percentage of
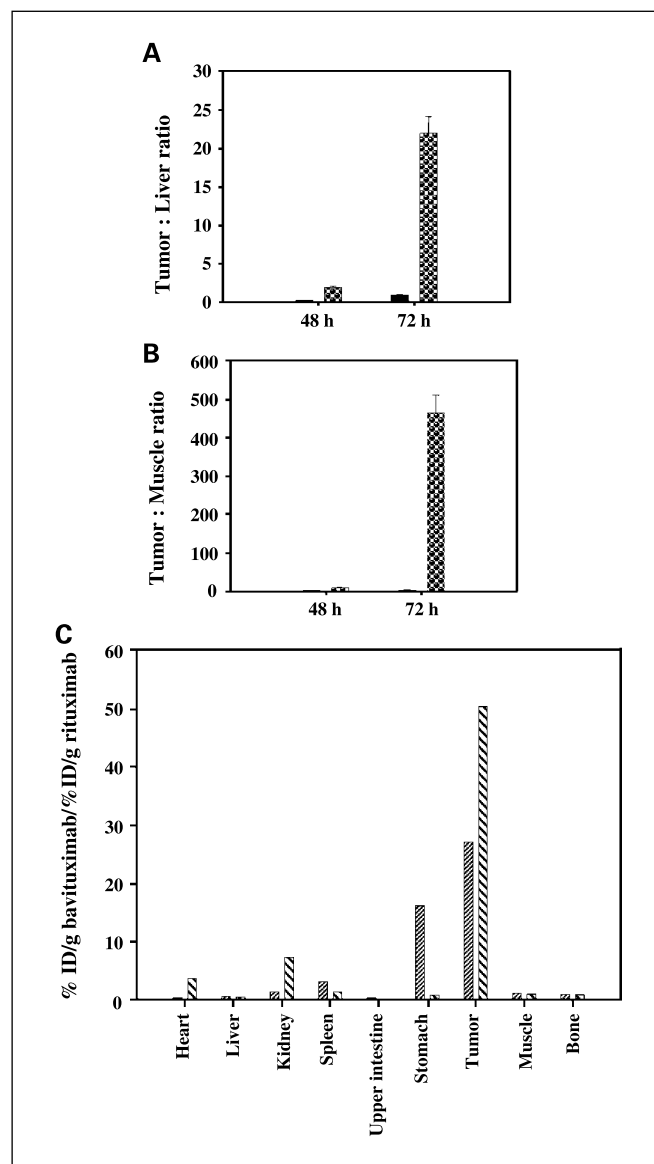
Fig. 2. Biodistribution. Dunning prostate R3327-AT1 tumor-bearing rats were injected with 185 kBq of [^{74}As]bavituximab or [^{74}As]rituximab i.v. Groups of four animals were sacrificed by exsanguination and perfusion 48 or 72 h after injection. *A,* tumor-to-liver ratios for rats sacrificed after 48 and 72 h after injection with [^{74}As]rituximab (*black*) or [^{74}As]bavituximab (*dots*). *B,* corresponding tumor to muscle ratios. *C,* specific localization of bavituximab/rituximab in major organs after 48 h (*narrow hatched*) and 72 h (*broad hatched*). Specific localization is calculated as the ratio of the % ID/gram for [^{74}As]bavituximab to the % ID/gram for [^{74}As]rituximab in tumor and normal tissues. At 72 h, the uptake of bavituximab was significantly higher in tumor than liver or muscle ($P < 0.001$).
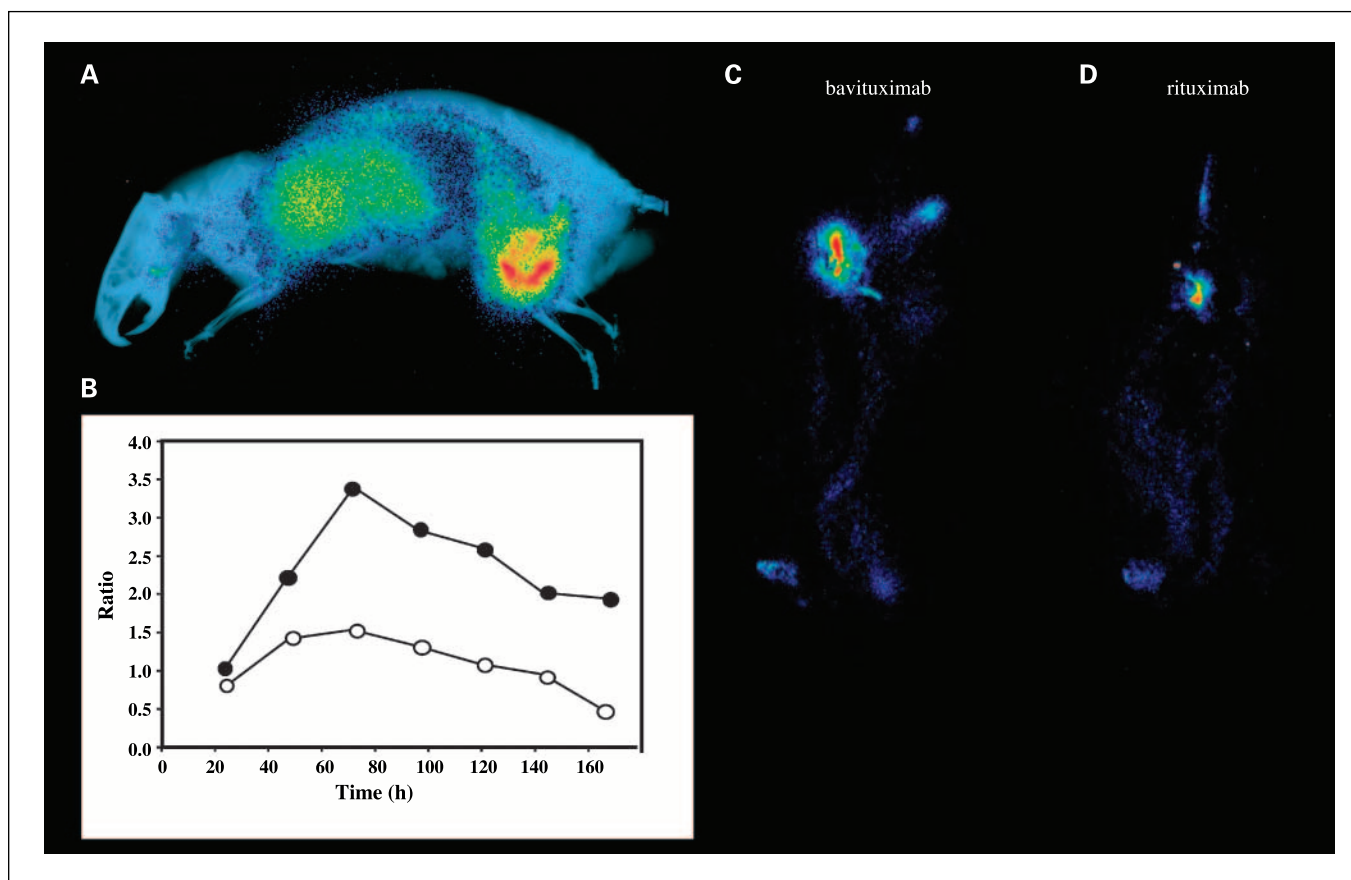
Fig. 3. Whole-body planar scintigraphy of Dunning prostate R3227-AT1 tumor-bearing rats. *A,* rats bearing ~20 mm diameter tumors were injected i.v. with 5 MBq of [^{74}As]bavituximab. The rats were imaged on a phosphor plate at various time points after injection. Representative image 72 h after injection. The image is overlaid on an X-ray picture to provide anatomic correlation. *B,* ratio of uptake of [^{74}As]bavituximab in tumor versus upper organs (liver, lung, heart) at various time points after injection. ●, outer tumor regions; ○, entire tumor. At 24 h after injection, no obvious contrast was observed, but at 48 h, the tumor became clearly visible and by 72 h, the tumor-to-organ ratio was the highest. *C-D,* scintigraphy of rats injected with 3 MBq [^{77}As]bavituximab or [^{77}As]rituximab (negative control). Images acquired with 30 min of exposure time at 72 h. Eight-fold higher uptake of bavituximab than of the control antibody was observed in the tumor.

the injected dose per gram of tumor was 0.25 and 0.65 for [^{74}As]bavituximab at 48 and 72 h, respectively. This level of localization is respectable given the inverse relationship between animal weight and % ID/gram in different species. Significant uptake of radioactivity was observed in the stomach 48 h after injection of [^{74}As]bavituximab but had decreased by 72 h. In most organs (heart, liver, kidney, muscle, bone), the two antibodies showed similar low uptake. Uptake of [^{74}As]labeled bavituximab and rituximab was observed in the spleen.

Figure 3A shows the whole-body scintigraphy of a representative rat imaged at 72 h after injection with [^{74}As]bavituximab. Figure 3B compares the radioactivity in the tumor to that in the upper organs (liver, lung, heart) at various time points after injection of [^{74}As]bavituximab. At 24 h, the tumor was barely distinguishable because of the high body background. At 48 h, the tumor was clearly localized, but some signal attributable to blood pool was observed in the upper organs. At 72 h, labeled bavituximab had substantially cleared from the blood and antibody localization to the tumor was most visible. Thereafter, tumor to background ratios declined. Images are also shown for rats injected with [^{77}As]bavituximab or [^{77}As]rituximab (Fig. 3C and D) and imaged 72 h after injection. Relatively little [^{77}As]rituximab (about one-eighth as much) localized to the

tumor compared with [^{77}As]bavituximab, showing that the localization of [^{77}As]bavituximab was antigen-specific.

Distribution of radioactivity within the tumor was heterogeneous. Slices of tumors were examined by autoradiography (Fig. 4). Extensive localization of [^{77}As]bavituximab was observed in the tumor periphery and throughout the central regions, although quite heterogeneously. For rituximab, activity was limited to the tumor periphery. PET images from a three-dimensional data set of a tumor-bearing rat obtained 48 h after injection of [^{74}As]bavituximab again showed strong localization to the tumor periphery with similar heterogeneity of activity in central regions (Fig. 5).

Frozen sections of tumor and normal tissues were stained for the presence of human immunoglobulin to identify the cells to which the bavituximab had localized. Sections were counter-stained with anti-rat CD31 to detect vascular endothelium (Fig. 6). The images were merged. Coincidence of staining between localized bavituximab and CD31 indicated specific localization of bavituximab to tumor endothelium (Fig. 6). Coincident staining was yellow, unless dominated by a particularly intense green or red fluorescence in that region. Labeled vessels were visible in all regions of the tumors with an average of 40 ± 10% labeled vessels. Labeled vessels were particularly abundant in and around regions of necrosis. Larger
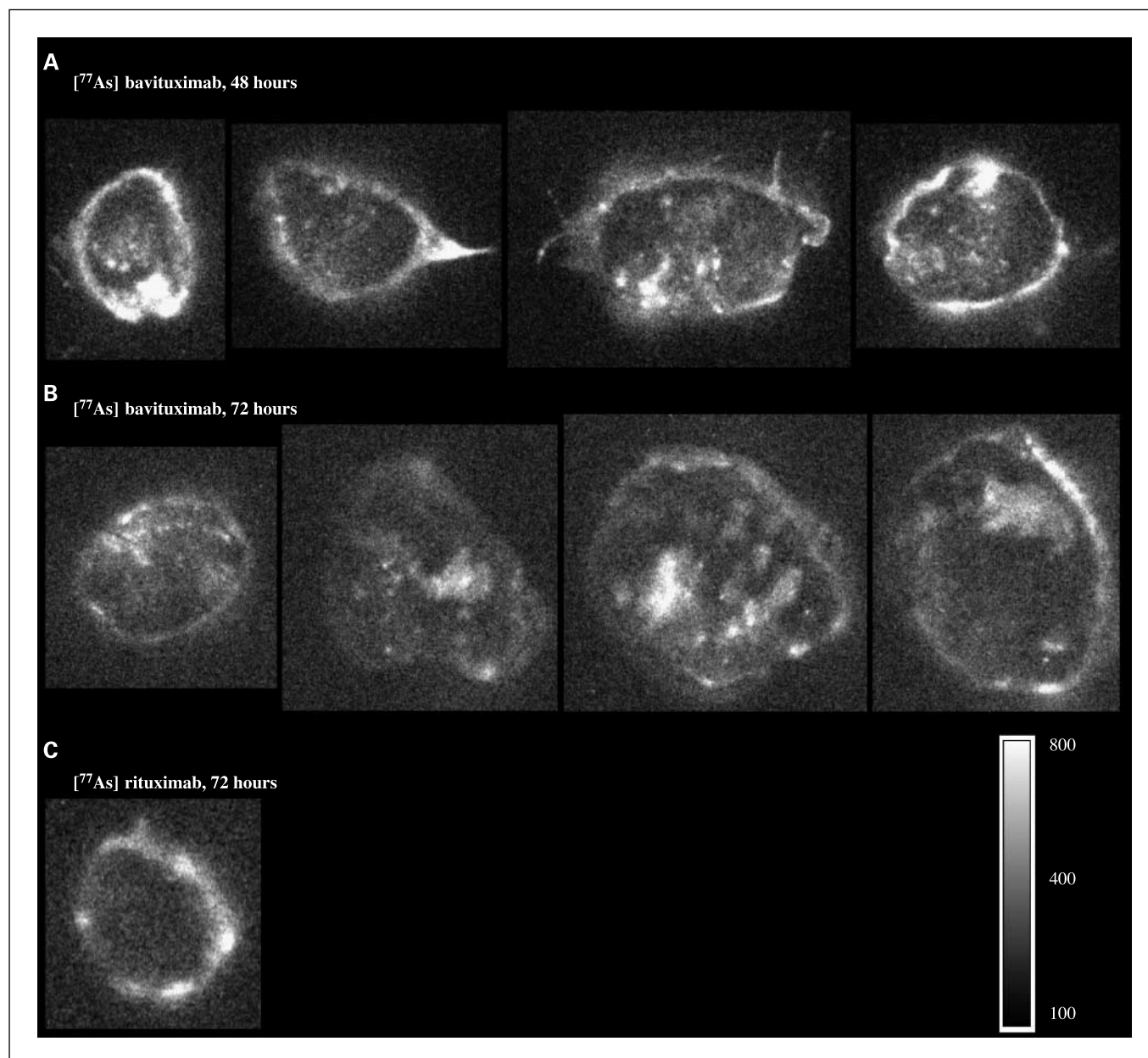
Fig. 4. Autoradiography of excised tumor sections. *A* and *B,* autoradiographs of 1-mm sections of Dunning prostate R3227-AT1 tumors from rats 48 or 72 h after injection with [^{77}As]bavituximab. Localization of bavituximab was observed in the tumor periphery and heterogeneously throughout the tumor core. *C,* [^{77}As]rituximab showed relatively little accumulation in the tumor, particularly in the central regions. The autoradiograph was exposed four times longer with [^{77}As]rituximab to visualize the distribution. Scale shows arbitrary storage phosphor units.

vessels sometimes had regions where the vascular endothelium was positive for localized bavituximab and other regions where it was not, showing heterogeneity of phosphatidylserine exposure within a single vessel. Regions where bavituximab had leaked into the tumor interstitium were also visible around the endothelium of some vessels. Nonvascular staining of dead and dying tumor cells in and around necrotic tumor regions was only occasionally observed. The antigen specificity of bavituximab localization to vessels was confirmed by the lack of endothelial cell staining in tumors from rats injected with rituximab. Localization of bavituximab to vascular endothelium in normal tissues was not detectable in rat heart, lung, liver, pancreas, kidney, spleen, brain, and testis.

Discussion

This study shows the feasibility of using arsenic radioisotopes to label a monoclonal antibody directed against anionic phospholipids on the surface of tumor vascular endothelium. Tumor selective targeting was observed *in vivo* and confirmed by biodistribution analysis and histology.

The two isotopes we selected for the present studies were ^{74}As, a potential clinical PET imaging isotope, and ^{77}As, a potential therapeutic isotope. ^{74}As (β^+, $T_{1/2}$ 17.8 days) has a long half life that allows imaging several days after administration of labeled antibody. Optimal tumor imaging in humans is often achieved 3 days or more after administration of a

labeled antibody, when the levels of free antibody have declined relative to those specifically bound or retained by the tumor (30, 31). ^{77}As (β^-, $T_{1/2}$ 38.8) has a high energy β^- emission suitable for antitumor therapy. Both isotopes, like other isotopes of arsenic, can be attached through stable covalent linkages to antibodies. In addition, arsenic does not accumulate in the thyroid or undergo transchelation to metal-binding blood and tissue proteins.

Jennewein and Rösch have developed efficient methods for isolating arsenic from irradiated germanium oxide targets to provide arsenic in a form that is useful for labeling sensitive biomolecules (7, 8). They have also developed novel methods for linking arsenic to biomolecules. Here, we show that monoclonal antibodies can be labeled efficiently with ^{74}As or ^{77}As to produce radioimmunoconjugates having full antigen-binding activity and high *in vitro* and *in vivo* stability. [*As]bavituximab was stable for several days when incubated in serum. Very little nonspecific uptake of radioactivity by the liver was seen in rats injected with [*As]bavituximab or [*As]rituximab, indicating that the labeled antibodies have high *in vivo* stability and that transfer of *As to serum proteins and uptake by the liver is minimal. This contrasts with the use of radioiodine for antibody labeling, where dehalogenation and high thyroid uptake are considerable. Instability is less of a problem for antibodies labeled with metal ions (e.g., ^{64}Cu) since the advent of improved chelating agents.

Biodistribution studies showed high selectivity of bavituximab toward tumor tissue. Within 48 h, the tumor to muscle ratio approached 10 and reached almost 500 by 72 h (Fig. 2).

The tumor to liver ratio exceeded 20 by 72 h. [^{74}As]bavituximab showed 30-fold to 50-fold higher absolute uptake in tumor than did the control antibody [^{74}As]rituximab. The *ex vivo* biodistribution matches the tumor uptake observed by imaging, with higher localization of bavituximab being seen in the tumor than in any normal tissues. Both *As-labeled bavituximab and rituximab accumulated in the spleen, possibly due to nonspecific capture of immunoglobulin or metabolites by the reticuloendothelial system. We did not observe preferential accumulation of [*As]bavituximab in the liver or spleen, which would be expected if bavituximab bound to phosphatidylserine-expressing blood cells being cleared by these organs.

The PET and planar scintigraphy studies showed pronounced localization of bavituximab to solid Dunning prostate R3227-AT1 tumors. Localization was seen in the periphery of the tumor and in various central regions, in agreement with prior PET studies with FDG or perfusion MRI (32–34). We have previously observed that phosphatidylserine-positive vessels are present in both the periphery and the core of tumors. It is likely that the peripheral location of the radioactivity seen with [*As]bavituximab in the present study is because this is the region of tumors that typically has the most abundant and functional blood supply. Some of the bavituximab was probably free in the blood of peripheral vessels or had diffused into peripheral tumor regions because a similar peripheral distribution was seen with the nonbinding rituximab control antibody. Heterogeneous localization of bavituximab was also observed throughout the central regions of the tumor. This central localization was antigen-specific because relatively little

Fig. 5. Small animal PET. *A* and *B,* small animal PET images obtained from a Dunning prostate R3227-AT1 tumor-bearing rat 48 h after injection of 10 MBq of [^{74}As]bavituximab coronal (*A*) and transaxial (*B*). PET intensity is overlaid on slices obtained by three-dimensional MRI. [^{74}As]bavituximab localized to the tumor (*arrows*) and was also visible in the blood pool of normal organs. The PET field of view (*FOV*) is indicated by the bracket. *C,* images of 1-mm sequential tumor slices from the three-dimensional data sets.
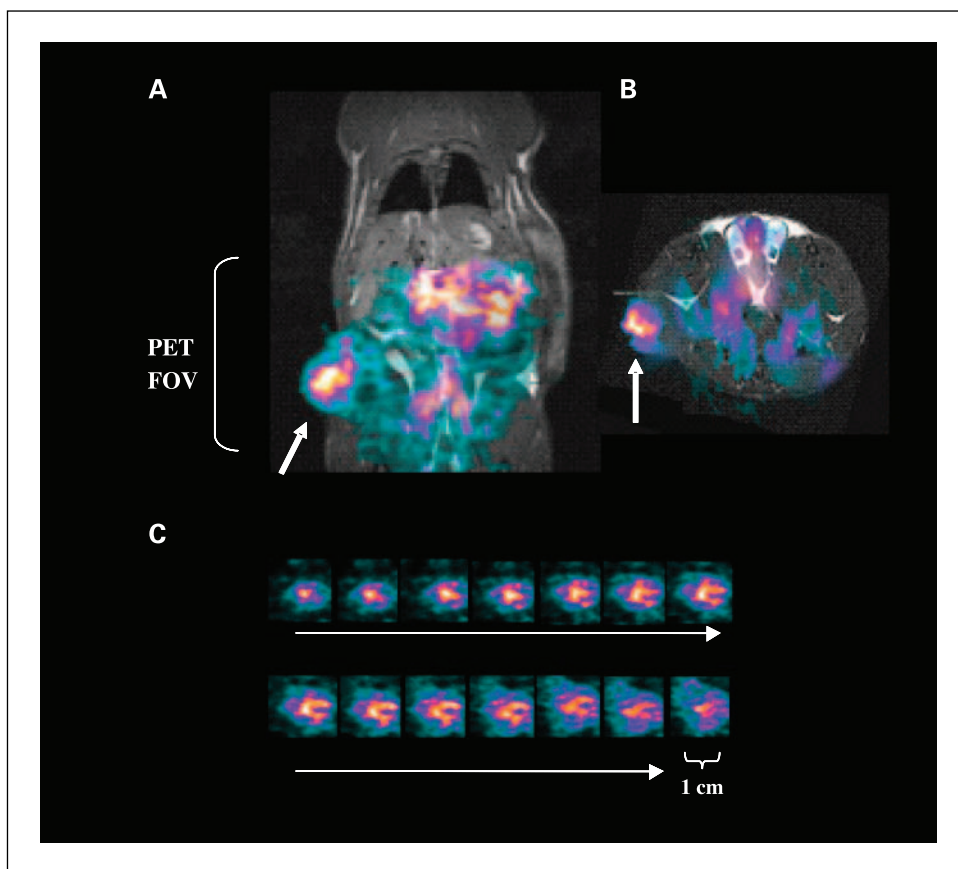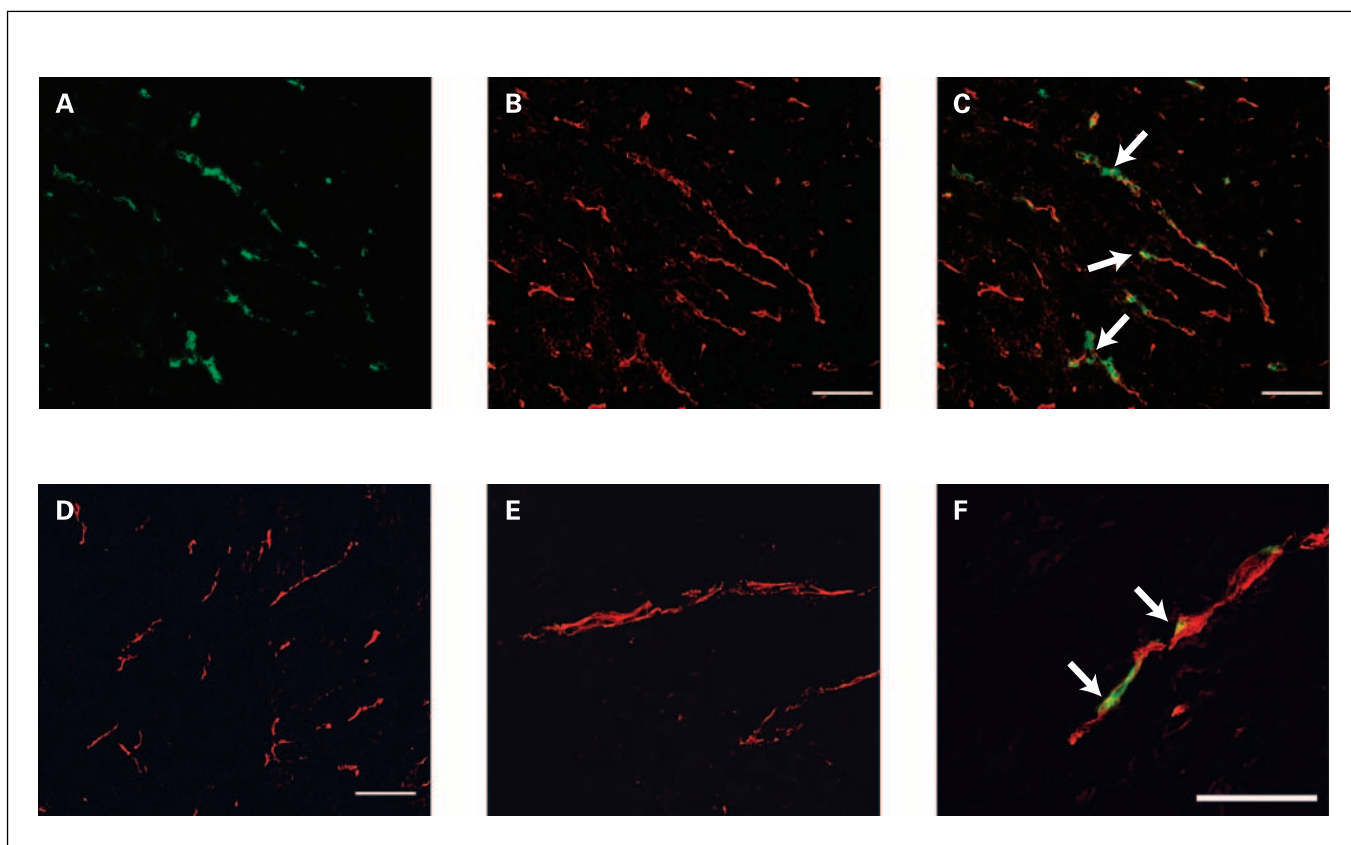
Fig. 6. Localization of bavituximab to tumor vessels after injection into rats bearing syngeneic Dunning R3227-AT1 prostate tumors. Rats were injected i.v. with bavituximab or rituximab. After 24 h, the rats were exsanguinated and their tumors were removed. *A-C* show blood vessels in a frozen section of tumor at low magnification. *A,* stained with biotinylated goat anti-human IgG followed by Cy2-streptavidin (*green*) to detect localized bavituximab; *B,* stained with mouse anti-rat CD31 followed by Cy3-labeled goat anti-mouse IgG (*red*) to detect vascular endothelium; *C,* a merged image of bavituximab localized on CD31-positive endothelium (*thick*). *D,* a merged image of blood vessels in the tumor of a rat injected with rituximab. No binding of rituximab was detected. *E-F,* higher magnification merged images of blood vessels in tumors from rats injected with rituximab (*E*) or bavituximab (*F*). *Bars,* 100 μm.

localization was seen in central tumor regions with the rituximab control antibody. Immunohistochemical examination confirmed that the bavituximab was bound to the endothelium of the central tumor regions with little staining of necrotic regions being visible. The heterogeneous staining with bavituximab is probably because some tumor regions have more hypoxia, acidity, or inflammatory cytokines than others, leading to variable levels of phosphatidylserine exposure on the tumor endothelium. We have previously examined multiple different types of mouse and human tumors growing in mice, and all have phosphatidylserine-expressing tumor vascular endothelium (10, 14, 35, 36). The percentage of phosphatidylserine-positive vessels ranged from 16% to 41%. Thus, we anticipate that vascular imaging observed with bavituximab in the present studies will extend to other tumor types. The Dunning prostate R3227-AT1 tumor has small areas of focal necrosis scattered throughout the tumor (37). The lack of strong localization of bavituximab to these necrotic regions could be related to difficulties of access associated with high interstitial pressure and inadequate lymphatic drainage. However, in a previous study using a different anti-phosphatidylserine antibody (9D2) and different tumors, staining of necrotic tumor tissue was observed in addition to the endothelium at later time points (10). The apparent difference in the ability of the two antibodies to localize to necrotic regions may relate

to idiosyncrasies of the tumor models or to differences in the ability of the two antibodies to resist proteolysis after binding. It is also possible that the cofactor protein β2-glycoprotein I, which is needed for phosphatidylserine binding by bavituximab but not 9D2, does not efficiently penetrate into extravascular tissues or is degraded rapidly by proteolytic enzymes within the tumor interstitium.

The present labeling chemistry can also be applied to other radioarsenic isotopes. [72]As has a half life of 26 h, suitable for imaging with antibody Fab′ and F(ab′)$_2$ fragments and other biomolecules having intermediate half lives. The abundance of positrons for [72]As is 88%, which is higher than in other commonly used positron emitters, such as [64]Cu (18.0% β$^+$, $T_{1/2}$ 12.7 h) or [124]I (23.0% β$^+$, $T_{1/2}$ 4.2 days). Arsenic provides two potentially therapeutic isotopes: [77]As ($T_{1/2}$ 38.8 h, $\bar{E}_{\beta^-}$ 226 keV), as used in the present study, and [76]As ($T_{1/2}$ 26.3 h, $\bar{E}_{\beta^-}$ 1.068 keV; see Supplementary Table S1). The multiple isotopes of arsenic potentially offer additional applications, such as combined imaging/dosimetry and radioimmunotherapy. Another advantage of arsenic is that, unlike iodine, it does not subject the thyroid to high irradiation. The doses of arsenic used for imaging with [[74]As]bavituximab are also several orders of magnitude below toxic levels, so that even if [74]As were released from the antibody, no toxicity would be expected. However, the arsenic isotopes do not include α emitters, which,

because of their short path length, could be advantageous for vascular targeted therapies.

In conclusion, we have exploited the unique properties of arsenic radioisotopes to achieve clear imaging of tumors with an antibody, bavituximab, directed against a tumor vessel marker. Radioarsenic-labeled bavituximab shows promise as a vascular imaging agent for tumor detection and dosimetry in man.

References

1. Rudin M, Weissleder R. Molecular imaging in drug discovery and development. Nat Rev Drug Discov 2003;2:123–31.

2. Massoud TF, Gambhir SS. Molecular imaging in living subjects: seeing fundamental biological processes in a new light. Genes Dev 2003;17:545–80.

3. Kumar R, Jana S. Positron emission tomography: an advanced nuclear medicine imaging technique from research to clinical practice. Methods Enzymol 2004; 385:3–19.

4. McQuade P, Rowland DJ, Lewis JS, Welch MJ. Positron-emitting isotopes produced on biomedical cyclotrons. Curr Med Chem 2005;12:807–18.

5. Boerman OC, Kopp MJ, Postema EJ, Corstens FH, Oyen WJ. Radionuclide therapy of cancer with radio-labeled antibodies. Curr Med Chem Anti-Canc Agents 2007;7:335–43.

6. Burnham CA, Aronow S, Brownell GL. A hybrid positron scanner. Phys Med Biol 1970;15:517–28.

7. Jennewein M, Qaim SM, Hermanne A, et al. A new method for the radiochemical separation of arsenic from reactor and cyclotron irradiated germanium oxide. Appl Rad Isoto 2005;63:343–51.

8. Jennewein M, Schmidt A, Novgorodov AF, Qaim SM, Roesch F. A no-carrier-added 72Se/72As radionuclide generator based on distillation. Radiochim Acta 2004;92:245–9.

9. Huang X, Bennett M, Thorpe PE. A monoclonal antibody that binds anionic phospholipids on tumor blood vessels enhances the antitumor effect of docetaxel on human breast tumors in mice. Cancer Res 2005;65: 4408–16.

10. Ran S, Downes A, Thorpe PE. Increased exposure of anionic phospholipids on the surface of tumor blood vessels. Cancer Res 2002;62:6132–40.

11. Ran S, Thorpe PE. Phosphatidylserine is a marker of tumor vasculature and a potential target for cancer imaging and therapy. Int J Radiat Oncol Biol Phys 2002; 54:1479–84.

12. Luster TA, He J, Huang X, et al. Plasma protein β-2-glycoprotein 1 mediates interaction between the anti-tumor monoclonal antibody 3G4 and anionic phospholipids on endothelial cells. J Biol Chem 2006;281:29863–71.

13. Ran S, Gao B, Duffy S, Watkins L, Rote N, Thorpe PE. Infarction of solid Hodgkin's tumors in mice by antibody-directed targeting of tissue factor to tumor vasculature. Cancer Res 1998;58:4646–53.

14. Ran S, He J, Huang X, Soares M, Scothorn D, Thorpe PE. Anti-tumor effects of a monoclonal antibody directed against anionic phospholipids on the surface of tumor blood vessels in mice. Clin Cancer Res 2005;11:1551–62.

15. Seigneuret M, Devaux PF. ATP-dependent asymmetric distribution of spin-labeled phospholipids in the erythrocyte membrane: relation to shape changes. Proc Natl Acad Sci U S A 1984;81: 3751–5.

16. Bombeli T, Karsan A, Tait JF, Harlan JM. Apoptotic vascular endothelial cells become procoagulant. Blood 1997;89:2429–42.

17. Boyle EM, Jr., Pohlman TH, Cornejo CJ, Verrier ED. Endothelial cell injury in cardiovascular surgery: ischemia-reperfusion. Ann Thorac Surg 1996;62: 1868–75.

18. Bevers EM, Comfurius P, Zwaal RF. Changes in membrane phospholipid distribution during platelet activation. Biochim Biophys Acta 1983;736:57–66.

19. Rote NS, Ng AK, Dostal-Johnson DA, Nicholson SL, Siekman R. Immunologic detection of phosphatidylserine externalization during thrombin-induced platelet activation. Clin Immunol Immunopathol 1993; 66:193–200.

20. Bitbol M, Fellmann P, Zachowski A, Devaux PF. Ion regulation of phosphatidylserine and phosphatidylethanolamine outside-inside translocation in human erythrocytes. Biochim Biophys Acta 1987;904: 268–82.

21. Zhao J, Zhou Q, Wiedmer T, Sims PJ. Level of expression of phospholipid scramblase regulates induced movement of phosphatidylserine to the cell surface. J Biol Chem 1998;273:6603–6.

22. Hamon Y, Broccardo C, Chambenoit O, et al. ABC1 promotes engulfment of apoptotic cells and transbilayer redistribution of phosphatidylserine. Nat Cell Biol 2000;2:399–406.

23. Pradhan D, Williamson P, Schlegel RA. Phosphatidylserine vesicles inhibit phagocytosis of erythrocytes with a symmetric transbilayer distribution of phospholipids. Mol Membr Biol 1994;11:181–7.

24. Balasubramanian K, Schroit AJ. Aminophospholipid asymmetry: a matter of life and death. Annu Rev Physiol 2003;65:701–34.

25. Duncan RJ, Weston PD, Wrigglesworth R. A new reagent which may be used to introduce sulfhydryl groups into proteins, and its use in the preparation of conjugates for immunoassay. Anal Biochem 1983; 132:68–73.

26. Henke K, Hartmann GH, Peschke P, Hahn EW. Stereotactic radiosurgery of the rat Dunning R3327-1 prostate tumor. Int J Radiat Oncol Biol Phys 1996;36: 385–91.

27. Zhao D, Ran S, Constantinescu A, Hahn EW, Mason RP. Tumor oxygen dynamics: correlation of in vivo MRI with histological findings. Neoplasia 2003;5:308–18.

28. Modestou M, Puig-Antich V, Korgaonkar C, Eapen A, Quelle DE. The alternative reading frame tumor suppressor inhibits growth through p21-dependent and p21-independent pathways. Cancer Res 2001;61: 3145–50.

29. Tsyganov EN, Anderson J, Arbique G, et al. UTSW small animal positron emission imager. IEEE Trans Nucl Inst 2006;53:2591–600.

30. Bischof Delaloye A, Delaloye B. Tumor imaging with monoclonal antibodies. Semin Nucl Med 1995;25: 144–64.

31. Von Kleist S. Ten years of tumor imaging with labelled antibodies. In vivo 1993;7:581–4.

32. Karam JA, Mason RP, Koeneman KS, Antich PP, Benaim EA, Hsieh JT. Molecular imaging in prostate cancer. J Cell Biochem 2003;90:473–83.

33. Jiang L, Zhao D, Constantinescu A, Mason RP. Comparison of BOLD contrast and Gd-DTPA dynamic contrast enhanced imaging in rat prostate tumor. Magn Reson Med 2004;51:953–60.

34. Zhao D, Jiang L, Hahn EW, Mason RP. Continuous low-dose (Metronomic) chemotherapy on rat prostate tumors evaluated using MRI in vivo and comparison with histology. Neoplasia 2005;7:678–87.

35. Beck AW, Luster TA, Miller AF, et al. Combination of a monoclonal anti-phosphatidylserine antibody with gemcitabine strongly inhibits the growth and metastasis of orthotopic pancreatic tumors. Int J Cancer 2006;118:2639–43.

36. He J, Luster TA, Thorpe PE. Radiation-enhanced vascular targeting of human lung cancers in mice with a monoclonal antibody that binds anionic phospholipids. Clin Cancer Res 2007;207:5211–8.

37. Hahn EW, Peschke P, Mason RP, Babcock EE, Antich PP. Isolated tumor growth in a surgically formed skin pedicle in the rat: a new tumor model for NMR studies. Magn Reson Imaging 1993;11: 1007–17.